Calcified Tissue International
https://doi.org/10.1007/s00223-018-0397-1

ORIGINAL RESEARCH

A Novel microCT Method for Bone and Marrow Adipose Tissue Alignment Identifies Key Differences Between Mandible and Tibia in Rats

Xavier Coutel[1] · Cécile Olejnik[1] · Pierre Marchandise[1] · Jérôme Delattre[1] · Hélène Béhal[2] · Greet Kerckhofs[3,4] · Guillaume Penel[1]

Received: 5 December 2017 / Accepted: 24 January 2018

Abstract

Bone homeostasis is influenced by the bone marrow adipose tissue (BMAT). BMAT distribution varies from one anatomical location in the skeleton to another. We developed an advanced microfocus computed tomography imaging and analysis protocol that allows accurate alignment of both the BMAT distribution and bone micro-architecture as well as calculation of the distance of the BMAT adipocytes from the bone surface. Using this protocol, we detected a different spatial BMAT distribution between the rat tibia and mandible: in the proximal metaphysis of the tibia a large amount of BMAT (~20% of the total BMAT) was located close to the bone surface (<20 µm), whereas in the alveolar ridge ~30% of the total BMAT was located between 40 and 60 µm from the bone surface. In the alveolar ridge of rats, the trabecular bone volume was 48.3% higher compared to the proximal metaphysis of the tibia ($p<0.0001$) and the percentage of adiposity determined to the relative marrow volume was lower (1.5%) compared to the proximal metaphysis of the tibia (9%, $p=0.0002$). Interestingly, in the tibia a negative correlation was found between the percentage of adiposity in the total volume and the trabecular thickness ($r=-0.74$, $p=0.037$). The present study highlights that in comparison to tibial proximal metaphysis, the mandibular bone exhibits a massive trabecular network and a low BMAT content with almost no contact with the bone surface. These findings are of great interest because of the importance of the fat–bone interaction and its potential relevance to several resorptive bone diseases.

Keywords Rats · Jaw bone · Osmium staining · Bone structure · Micro-computed tomography imaging · Adipocytes

Introduction

Through the last decades, adipose tissues have revealed their diversity regarding their cellular composition, anatomical location and physiopathological properties [1, 2]. Among the fat depots, bone marrow adipose tissue (BMAT) emerges as a distinct fat depot regarding the size, distribution and metabolic function of the marrow adipocytes [3–5]. The presence of this adipose tissue and its normal age-related conversion in the bone marrow was a long-standing knowledge thanks to histomorphometry and magnetic resonance imaging (MRI) but has been surprisingly disregarded in the craniofacial skeleton. Distribution of the BMAT in the skeleton is a tightly regulated process with skeletal site specificities [6–8].

Recently, in rodents, BMAT content and composition have been reported to be differently distributed between the distal and the proximal metaphysis in the tibia. But the

✉ Xavier Coutel
xavier.coutel@univ-lille2.fr

1 Univ.Lille, Univ. Littoral Côte d'Opale, EA 4490 - PMOI – Physiopathologie des Maladies Osseuses Inflammatoires, 59000 Lille, France

2 Univ. Lille, CHU Lille, EA 2694 - Santé publique: épidémiologie et qualité des soins, Unité de Méthodologie et Biostatistiques, 59000 Lille, France

3 Department of Development and Regeneration, Skeletal Biology and Engineering Center, KU Leuven, Leuven, Belgium

4 Prometheus, Division of Skeletal Tissue Engineering, KU Leuven, Leuven, Belgium

Published online: 30 January 2018

status of the mandible is still not clear. In the jaws, two functional areas characterized by a high bone remodeling activity have been identified in rats: the alveolar ridge and the condyle [9]. Yamada et al. established that the conversion of hematopoietic to fatty marrow in young subjects occurs first in the mandibular corpus followed by the ramus and finally the condyle [10]. The BMAT content within the alveolar ridge remains to be elucidated on adults and the influence of the teeth on the alveolar ridge BMAT content have not been evaluated to date. Lack of knowledge regarding the BMAT location and composition in the craniofacial skeleton particularly in presence or absence of the teeth impairs our understanding of not only bone homeostasis during aging but also a broad range of pathological conditions including periodontal diseases.

Although BMAT origin, development and function are still being determined, its importance in bone–fat interactions remains of high clinical interest [11–13]. From clinical findings, marrow fat composition also plays a role in skeletal homeostasis [14–16]. Recent studies in both human and animal models indicate a relationship between the amount of BMAT and several bone diseases [17–19]. BMAT is also involved in the regulation of hematopoiesis [20] and modified during aging [21]. Through aging, an increase of BMAT content was observed and appears to be inversely correlated to decrease trabecular bone volume in iliac crest [22]. The bone remodeling activity seems to be modulated by the local bone marrow microenvironment adjacent to bone surface [23, 24]. Consistent with the importance of paracrine signaling of BMAT, in vitro co-culture studies from our lab by Clabaut et al. suggest that adipocytes may affect bone cells fate by promoting trans-differentiation (or re-programming) of osteogenic cells [25]. Li et al. reported also histomorphometric data in vertebrae and concluded that skeletal sites with high yellow marrow fat content, such as caudal vertebrae or distal tibiae, did not induce cancellous bone osteopenia [26]. Given this variability, to understand bone–fat interactions, the relationship between bone and BMAT proximity deserves careful consideration especially among bone sites.

The anatomical dissemination and the difficulties to access BMAT still hamper our understanding of the relative involvement of BMAT in health and diseases. The aim of the present study was to develop an original microCT imaging and analysis protocol that combines two registered microCT scans of the same sample from which both the micro-architecture and the BMAT content (using osmium tetroxide staining) can be calculated. This novel protocol allowed to establish the BMAT status of both the mandibular alveolar ridge and condyle compared with the tibial metaphysis in a rat model. Moreover, and uniquely, it allowed to investigate the distance between BMAT and trabecular bone surface.

Materials and Methods

Animal Procedures

Six-month-old female Sprague–dawley rats ($n=9$) with a homogeneous weight of 361 g ($\pm$18 g, SD) were provided by Janvier Lab (Laval, France). The provider reports that the rats were free of known viral, bacterial and parasitic pathogens, in accordance with the approval obtained by the Veterinary Department of the French Ministry of Agriculture (Approval No. B 53-103-02). All experiments on animals were carried out in an accredited animal facility (Authorization No. B5935010) at the University of Lille under the approval of the Animal Ethic Committee and in accordance with the directive 2010/63/EU and the "Principles of Laboratory Animal Care" recommended by the National Society for Biomedical Research in France. Rats ($n=3$/cage) were housed in type 4 cages filled with Lignocel® (hygiene animal bedding) enriched with horizontal tubes for climbing under controlled conditions at 22 $\pm$ 2 °C on a 12 h light/12 h dark cycle with lights on from 7.00 a.m. to 7.00 p.m. They were fed ad libitum (free access to tap water and standard chow diet). Rats were euthanized by exsanguinations under anesthesia at 6 months. At killing, right hemi-mandibles and tibias were harvested, immediately fixed for 48 h in 10% neutral-buffered formalin and stored in phosphate buffered saline prior to further analyses.

MicroCT Image Acquisition and Reconstruction: Scan 1

To assess simultaneously the bone micro-architecture and the BMAT content, the trabecular area was investigated in three skeletal locations: (i) the intra-radicular tooth-bearing (alveolar) bone of the first molar, (ii) the central area of the mandibular condyle in the mandibles and (iii) the secondary spongiosa of the tibial metaphysis (Fig. 1).

All bone samples were scanned a first time (i.e. SCAN1) to allow analysis of the trabecular bone morphometric parameters. Specimens (mandibles and tibiae) were placed in a plastic sample holder and were scanned using a Skyscan 1172 microCT device (Bruker MicroCT, Kontich, Belgium). The software suite provided by the manufacturer was used for image acquisition, reconstruction, analysis and 3D visualization (Skyscan 1172©, NRecon©, Dataviewer, CTAn©, CTVox™).

Scan settings were as follows: isotropic voxel size 10 µm^3, 80 kVp, 100 µA, Al–Cu filter, 2400 ms integration time, 0.5° rotation step over 180°.

For the reconstruction (NRecon©), the following settings were applied to clearly distinguish the mineralized

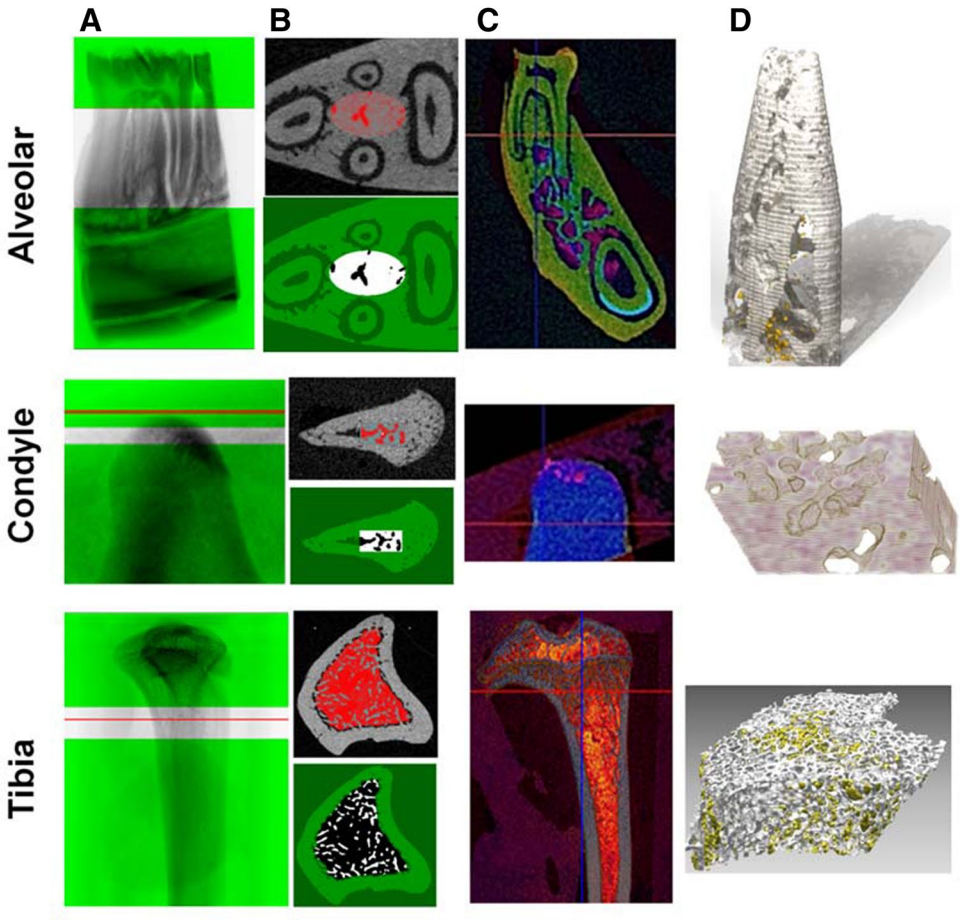

Fig. 1 Global approach to co-investigate the trabecular bone micro-architecture and the BMAT in the mandible (alveolar and condylar bone) and in the tibia. **a** Shadow projections showing the volume of interest. **b** Cross-sections illustrating the trabecular ROI and the corresponding cross-section after binarization of the trabecular network. **c** Registration of SCAN1 and SCAN2 datasets. **d** 3D rendering of the trabecular bone network (white) and BMAT (yellow) within the ROI. (Color figure online)

compartment of the bone from the bone marrow: Gaussian smoothing, ring artifact reduction 6, beam hardening correction 50%.

Osmium Tetroxide Staining Protocol

After these first acquisitions, samples were prepared for BMAT analysis. Thus, all the bone samples were decalcified under controlled slow oscillations in 4% formic acid/10% NBF (1:1), pH 7.4, for 4 days. Once demineralized, they were rinsed in distilled water. Each decalcified bone was then stained in the fume hood for 48 h in a 45 ml staining solution that was composed of a 1% osmium tetroxide solution stabilized in a 2.5% dichromate potassium solution at room temperature. Then, the bones were washed, in the same tube, by removing the staining solution and soaking the stained bones in 45 ml of PBS for 3 h at room temperature. This washing step was repeated twice and the last wash was left in the hood overnight. Osmium stained bones were then moved to a fresh set of 50 ml falcon tubes containing 45 ml of PBS each and were stored at + 4 °C until microCT acquisition.

MicroCT Image Acquisition and Reconstruction: Scan 2

After osmium tetroxide staining, the decalcified and stained bone samples were scanned a second time (i.e. SCAN2) to allow analysis of the BMAT.

Samples were scanned using the same acquisition settings as for the first scan.

For the reconstruction of the SCAN2 datasets, the following settings were applied to reveal osmium-stained BMAT: Gaussian smoothing, ring artifact reduction 3, beam hardening correction 30%.

Image Datasets Alignment (SCAN1 and SCAN2 Registration)

The SCAN1 and SCAN2 datasets were rotated to obtain the same orientation, which was specific for each skeletal location (the longitudinal axis of the proximal metaphysis in the tibia and the mandibular condyle and the first molar in the alveolar ridge for the mandible, see Fig. 1). Then, the reoriented datasets of each sample (SCAN1 as reference, SCAN2 as target) were manually registered using Dataviewer

software (v. 1.5.2.4) following these critical steps: (i) co-registration of the global outlines; (ii) adjustment of the enamel of the rodent incisor (in case of the alveolar ridge) and (iii) progressive adjustment of the trabecular network and bone marrow space using the profile scale diagram and different angles of view (Fig. 1).

Determination of the Regions of Interest (ROI)

After registration, regions of interest (ROI) were drawn in the SCAN1 datasets that delineated the trabecular area of the samples using CTAn. For the alveolar ridge, ROIs were selected as the intra-radicular bone of the first molar from the furcation to the apex roots, as adapted from the protocol of Du et al. (modification: oval shape instead of a circular one) [27]. In the condyle, the ROI was selected according to the method described by Jiao et al. as a rectangle shape (1 mm length, 0.5 mm height) in the central compartment (Fig. 1) [28]. In the proximal tibia, 200 cross-sections (2 mm height) were selected 1.5 mm under the growth plate and the trabecular area was isolated from the cortical area by a semi-automated protocol in CTAn© [29].

MicroCT Image analysis: trabecular Bone Micro-architecture

In these ROIs of the SCAN 1 datasets, a one-level Otsu's method was used to determine the threshold between the mineralized tissue and the bone marrow compartment (and vice versa) [30], and the following bone microstructural parameters, reflecting the morphology of the trabecular network for each skeletal location, were measured using CTAn©: percent bone volume (BV/TV, %), percent marrow volume (Ma.V/TV, %), trabecular bone surface/volume ratio (BS/TV, mm^{-1}), trabecular number (Tb.N, mm^{-1}), trabecular thickness (Tb.Th, mm), trabecular separation (Tb.Sp, mm) and trabecular pattern factor (Tb.Pf, mm^{-1}).

MicroCT Image analysis: BMAT Content and Distribution

For quantification of the BMAT content, each defined ROI of the SCANS 1 datasets was re-used on the co-registered SCAN2 dataset to determine the BMAT content in the same area as where the bone micro-architecture was assessed. For the mandibular bone, a fixed threshold value (between 110 and 255 Gyscale levels) was used for both skeletal locations. In the tibia, the BMAT was segmented using a multilevel Otsu algorithm (3 levels). The following BMAT parameters were measured for each skeletal location: percentage of adipocyte volume in the total volume of the ROI (Ad.V/TV, %) and, in an original way, the ratio adipocyte volume/marrow volume (Ad.V/Ma.V, %) which constitute a novel 3D parameter. To assess the spatial distribution profile of BMAT in relation to the bone surface, a customized stepwise process (i.e. task list) was created in CTAn© to plot the percentage of adiposity versus the distance from the trabecular bone surface. This task list combines, after uploading the segmented osmium stained BMAT from the SCAN2 datasets as the image and the binarized trabecular network of the SCAN1 datasets as ROI,

1. one-level Otsu thresholding,
2. morphological operation: 20 µm 3D dilatation step (2 pixels),
3. saving images,
4. 3D morphological analysis to determine the percentage of adiposity in this volume.

Based on the trabecular separation parameter, these four tasks have been repeated seven times to cover the entire marrow cavity.

Statistical Analyses

All statistical methods were performed with SAS software package, release 9.4 (SAS Institute, Cary, NC). Data are presented as mean ± standard deviation (SD). Normality of distributions was assessed graphically and using the Shapiro–Wilk test.

Comparison between the three skeletal locations was made using a linear mixed model to take into account the correlation between the repeated measures within subjects (one measure per location) by including a random subject effect. Post-hoc pairwise comparisons between skeletal locations were performed. Residuals of the model were checked.

Relationship between trabecular bone micro-architecture and BMAT content was assessed using a linear mixed model to take into account the correlation between the repeated measures within subjects. This model included interaction term between the location and the distance of trabecular bone surface. If significant interaction was observed, difference between each site was assessed at each distance of trabecular bone surface using linear contrasts.

Correlation between variables was examined among each site by a Spearman's rank correlation coefficient. Statistical significance for all above tests was set at $p < 0.05$.

Results

Our novel microCT imaging and analysis protocol allowed accurate and simultaneous characterization of the trabecular bone micro-architecture and the BMAT content and spatial distribution within the same anatomical location (Fig. 1). Three skeletal sites (alveolar ridge, condyle and proximal

tibia) in rats have been investigated by this approach in the present study.

Trabecular Bone Micro-architecture

Micro-architectural differences were found between the three skeletal locations (Fig. 2). More specifically, BV.TV was 48.3% higher in the alveolar ridge and 58.2% higher in the condyle compared to tibial metaphysis. Tb.N was 20.9% higher in the alveolar ridge and 24.1% higher in the condyle compared to the tibial metaphysis, and this was associated with an increased mean trabecular thickness of 38.5% in the alveolar ridge and 46.7% in the condyle compared to tibia. Tb.Sp was similar for the alveolar ridge and the tibial metaphysis, whereas the condyle exhibited a mean trabecular separation that was 81.8% higher than that of the tibial metaphysis. Tb.Pf was negative in the alveolar ridge and in the condyle while it was found to be positive in the tibia. BS/TV was found to be ~40% inferior in the alveolar ridge and the condyle in comparison with tibial metaphysis.

BMAT Content

BMAT content in relation to the trabecular bone was obtained using our novel microCT imaging and analysis protocol as shown in Fig. 1d. The alveolar ridge showed a Ma.V/TV ratio that was 77.5% lower than that of the tibial metaphysis. The condyle exhibited an even higher difference compared to the tibial metaphysis (−185%, $p<0.0001$). No BMAT was observed in the condyle (Fig. 3). In the tibial metaphysis, the percentage of adipocyte volume was higher compared to the alveolar ridge both when determined relative to the total volume (6% vs 0.5%, $p<0.0001$) as to the marrow volume (9% vs 1.5%, $p=0.0002$).

Correlation and Spatial Relationship Between the Trabecular Bone and the BMAT

A negative correlation was found in the tibia between the adipose volume/total volume ratio and the trabecular thickness ($r=-0.74$, $p=0.037$). For the two other skeletal locations, no significant correlations were found between the

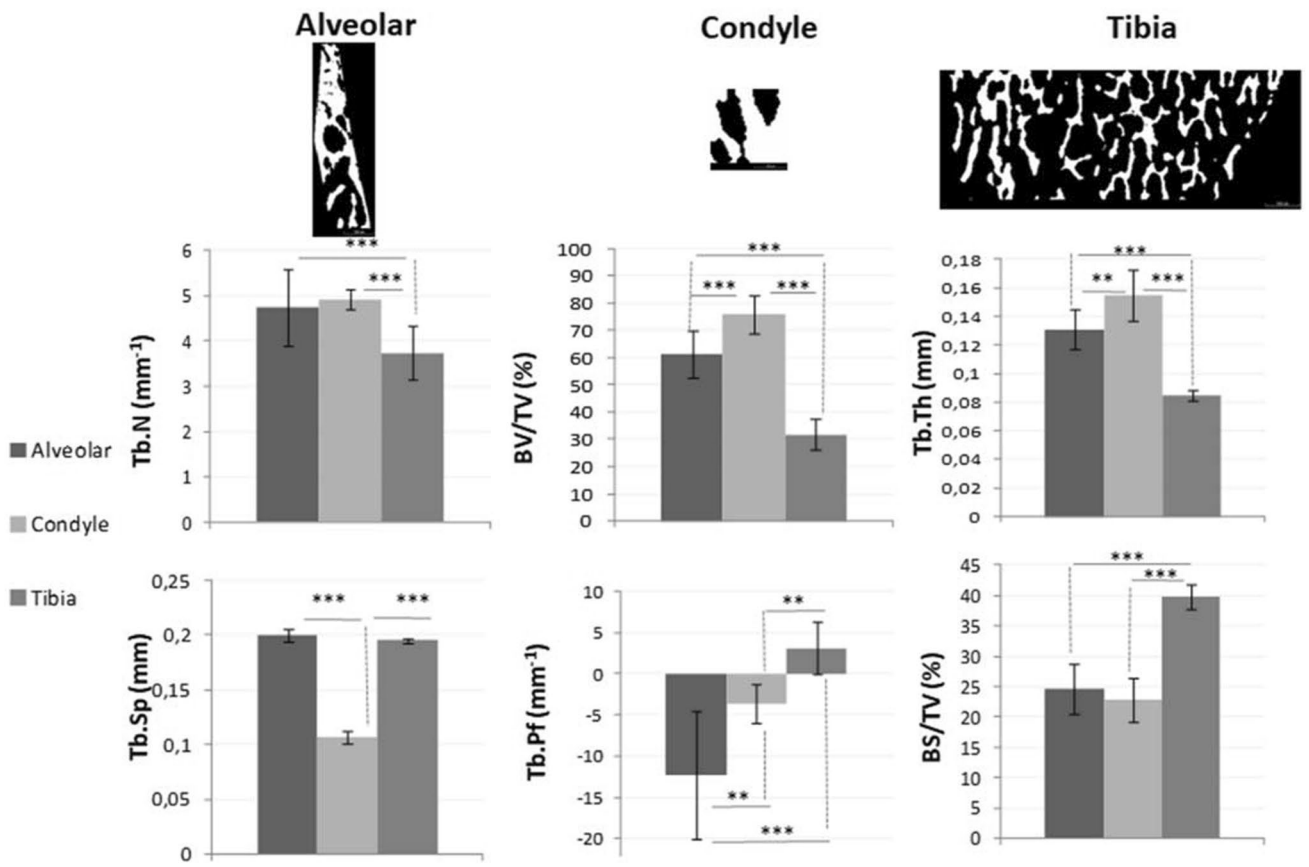

Fig. 2 Trabecular morphometric parameters (histograms) and representative 2D binarized sagittal cross-sections showing trabecular bone (white) and marrow cavities (black) in the three skeletal locations: *BV/TV* trabecular bone volume/total volume ratio (%), *Tb.N* trabecular number (mm^{-1}), *Tb.Th* trabecular thickness (mm), *Tb.Sp* trabecular separation (mm), *Tb.Pf* trabecular pattern factor (mm^{-1}), *BS/TV* bone surface/total volume ratio (mm^{-1}); $^{**}p<0.01$, $^{***}p<0.0001$

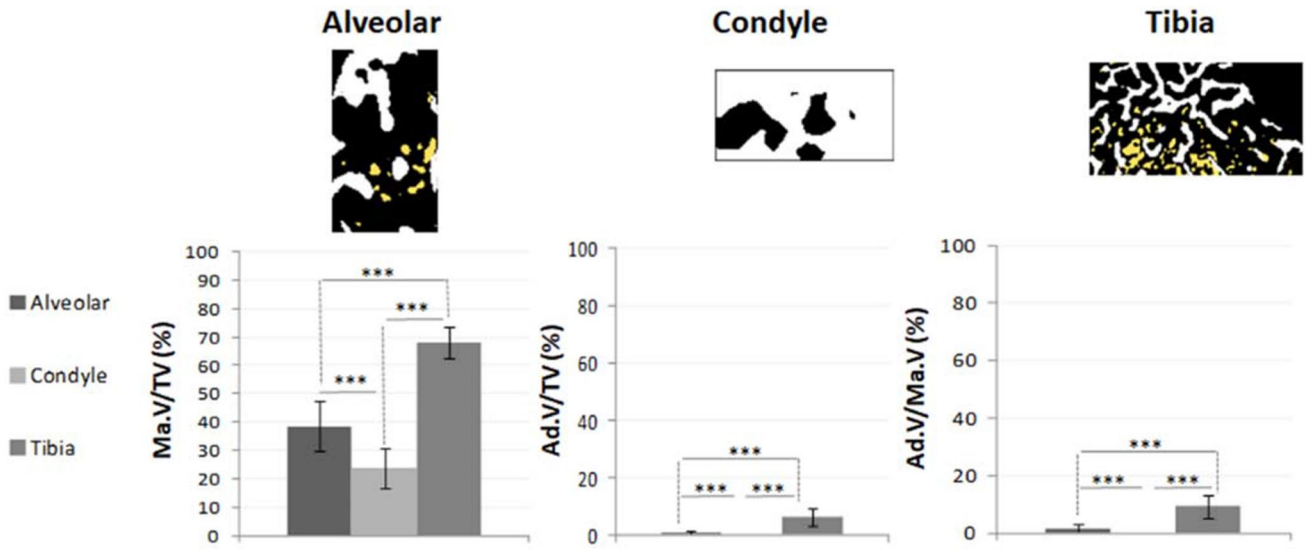

Fig. 3 Bone marrow adipose properties (histograms) and representative co-localisation of trabecular bone (white) and marrow adiposity (yellow) in 2D horizontal cross-sections after registration in the three skeletal locations: *Ma.V/TV* marrow volume/total volume ratio (%), *Ad.V/TV* adipose volume/total volume ratio (%), *Ad.V/Ma.V* adipose volume/marrow volume ratio (%); $^{**}p < 0.001$, $^{***}p < 0.0001$. (Color figure online)

bone micro-architecture and the BMAT content. Our novel microCT imaging and analysis protocol uniquely allowed to assess the spatial relationship between the bone and the BMAT. No assessment of this spatial relationship was possible for the condyle, since there was no BMAT present in this location. In both the other skeletal locations, i.e. the alveolar ridge and the tibial metaphysis, it was seen that 50% of the adipocyte volume was located at a mean distance of 40 µm from the trabecular bone surface (Fig. 4a). Interestingly, in the tibial metaphysis there were more adipocytes located close to the trabecular surface (~25% located at 20 µm; Fig. 4b) than in the alveolar ridge (~30% located between 40 and 60 µm; Fig. 4b). Significant differences were found until 60 µm.

Discussion

The rat model is considered as a suitable model for assessing the bone micro-architecture for many applications [31, 32]. The choice of the age is, however, crucial as the impact of skeletal maturation could impair the results. Rats experience a natural permanent skeletal growth until 6 months of age [33–35]. Therefore, 6 months is often reported in the

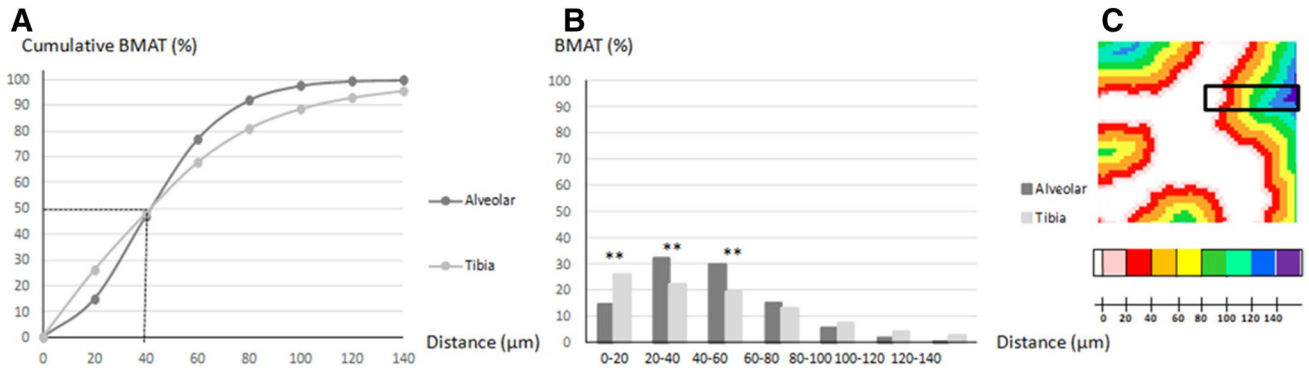

Fig. 4 Spatial relationship between the trabecular bone surface and the BMAT. **a** Cumulative percent of the BMAT in function of the distance to the trabecular bone surface. **b** Distribution histogram of the BMAT content in the alveolar ridge and the tibial metaphysis in function of the distance to the trabecular bone surface. **c** Representative image illustrating the novel approach of progressive dilatation of the trabecular bone network used as ROI to quantify the mean distance separating bone from adipose depots (color code), the white representing the bone trabeculae without any dilatation of the ROI. (Color figure online)

recent literature as an accurate period to investigate bone or bone marrow changes so as to avoid any confounding factors due to growth or senescence. Since also the BMAT content is age-related, the age is an important aspect that has been taken into account in the present study, which assesses both the BMAT and the bone micro-architecture. Therefore, 6-month-old rats have been selected for our study.

The present data showed skeletal location-related differences in the bone micro-architecture.

Indeed, a much denser bone micro-architecture was observed in the mandible (> 50% in trabecular bone volume, > 20% in trabecular number, > 40% in trabecular thickness) compared to the tibial metaphysis. In addition, the negative trabecular pattern factor values indicate a more connected trabecular lattice and a prevalence of enclosed cavities with concave surfaces in the mandible while positive value indicates a more disconnected trabecular structure in the tibial metaphysis. BS/TV parameter, representing the specific surface, have been described as a good predictor of bone loss [36]. The higher value in the tibial metaphysis may explain its more sensitive response to bone loss in comparison to the jaws. Bone loss was found to be enhanced preferentially within limb in ovariectomized (OVX) animals studies. In normal protein diet–fed animals, OVX led to a reduction of BV/TV of 4.9% in the mandible but 82% in the tibia ($p < 0.001$) [37]. Elovic et al. reported that in the mandible of adult rats (~ 4 months), OVX led to a 15 and 28% increase in failure load and stiffness, respectively, but no change in bone area fraction or bone mineral density. In older rats (~ 6 months), OVX led to an 8% decrease in bone area fraction, but no change in failure load, stiffness, or bone mineral density of the mandible [38, 39]. In human, clinical situations of bone loss such as osteoporosis, the relationship between mandibular alteration and prediction of osteoporotic fracture is controversial and of low sensitivity [40, 41]. These site-skeletal differences could be in part explained by the masticatory activity, resulting in cyclic loads on the mandibular teeth-bearing bone compared to the long bones in animals [42, 43]. A higher bone turnover rate has also been reported in the jaws [9, 44].

The amount of trabecular bone was the highest in the condyle, with a mean trabecular volume of about 75%, followed by the alveolar ridge (61.5%) and finally the tibial metaphysis (32%). This higher bone volume in the condyle is associated with a higher mean trabecular density and thickness and a mean inter-trabecular distance that is twice less compared to the tibia or the alveolar ridge. These results are consistent with those of Choi et al., who reported a denser microstructure in the condyle according to the presence or the absence of teeth in posterior sectors [45, 46]. Bresin et al. suggested that the continuously erupting incisor in the rat, which occupies a large part of the mandibular body, may also play a role in the micro-architecture of the teeth-bearing area [47]. However, in the present study, the ROI in which the bone micro-architecture was analyzed was chosen in a distant area from the incisor (inter-radicular bone of the first molar).

In terms of bone micro-architecture, the reported findings are in accordance with previous studies that focused on skeletal specificities [37], but they provide for the first time new information on the spatial distribution of BMAT in the mandible of mature rats. Using our novel microCT approach, we detected a different spatial BMAT distribution between the rat tibia and mandible: in the proximal metaphysis of the tibia a large amount of BMAT (~ 20% of the total BMAT) was located close to the bone surface (< 20 µm), whereas in the alveolar ridge ~ 30% of the total BMAT was located between 40 and 60 µm from the bone surface. Interestingly, in the tibia a negative correlation was found between the percentage of adiposity in the total volume and the trabecular thickness ($r = -0.74$, $p = 0.037$). No BMAT was observed in the condyle of the 6-month-old female rats. This is in correspondence with the human study of Yamada et al., in which later marrow adipose conversion is described in the condyle compared to the mandibular body [10].

Quantification of BMAT in animals (mainly mice) was first estimated by counting lipidic droplet cells on 2D histological sections. However, it was time-consuming, resource intensive and most of all inconsistent between laboratories as it may miss changes in 3D BMAT content. More recently, BMAT volume and heterogeneity was assessed by 3D approaches using microCT imaging to better understand the BMAT development, function and implication in bone diseases and treatment [21, 22]. However, the available studies present several limitations in the characterization of BMAT in relation to the bone surface and structure (i.e. no possible measurement of BMAT content regarding to the marrow volume, no determination of the spatial distribution of the BMAT and no quantification of both bone micro-architecture and BMAT within the same region of interest). To our best knowledge, this is the first study to allow an accurate characterization of both the BMAT distribution and bone micro-architecture (after image datasets alignment) as well as calculation of the distance of the BMAT adipocytes from the bone surface. Taken together, the results of the present study report that mandibular bone has a denser bone micro-architecture compared to the tibial metaphysis, a lower bone marrow volume and a BMAT content located at distance from the trabecular bone surface.

Conclusion

Investigating and understanding the relationship between BMAT and bone quality has emerged as an exciting area of research. As pointed out by other groups, one should take

into account the fat content in the marrow when assessing bone integrity as it may affect bone microstructure [48, 49]. BMAT has turned to be a heterogeneous fat depot whose adipocytes diverge in their phenotype and their response to stimuli according to their location in bone and its marrow environment [3]. With the help of a novel method aligning the bone and the BMAT in 3D, the present study establishes the BMAT content and distribution in alveolar and condyle sites of rat mandible. These results are crucial to have a better understanding of mandibular specific response during various physiopathological events that should be investigated with rat model.

Acknowledgements The authors thank the staff of the animal care facility (DHURE, Lille, France) for supplying the help on surgical procedures. This study was supported by the French Society of Rheumatology (SFR). GK acknowledges the Research Foundation—Flanders for her postdoctoral Grant (FWO/12R4315N) and her travel grant for a 6-months stay abroad in the PMOI lab.

Author Contributions GP, CO, XC conceived and designed the experiments. XC, CO, PM, JD, GK performed the experiments (acquisition, analysis and/or interpretation of the data). XC drafted the manuscript. All authors critically revised the article and approved the final manuscript.

Funding This study was supported by the French Society of Rheumatology.

Compliance with Ethical Standards

Conflict of interest Xavier Coutel, Cécile Olejnik, Pierre Marchandise, Jérôme Delattre, Hélène Béhal, Greet Kerckhofs, and Guillaume Penel declare that they have no conflict of interest.

Human and Animal Rights and Informed Consent All applicable international, national, and institutional guidelines for the care and use of animals were followed.

References

1. Rosen ED, Spiegelman BM (2014) What we talk about when we talk about fat. Cell 156:20–44. https://doi.org/10.1016/j.cell.2013.12.012
2. Lanske B, Rosen C (2017) Bone marrow adipose tissue: the first 40 years. J Bone Miner Res 32:1153–1156. https://doi.org/10.1002/jbmr.3140
3. Hardouin P, Marie PJ, Rosen CJ (2016) New insights into bone marrow adipocytes: report from the first European meeting on bone marrow adiposity (BMA 2015). Bone 93:212–215. https://doi.org/10.1016/j.bone.2015.11.013
4. van der Eerden B, van Wijnen A (2017) Meeting report of the 2016 bone marrow adiposity meeting. Adipocyte. https://doi.org/10.1080/21623945.2017.1313374
5. Scheller EL, Rosen CJ (2014) What's the matter with MAT? Marrow adipose tissue, metabolism, and skeletal health. Ann N Y Acad Sci 1311:14–30. https://doi.org/10.1111/nyas.12327
6. Craft CS, Scheller EL (2016) Evolution of the marrow adipose tissue microenvironment. Calcif Tissue Int 1–15. https://doi.org/10.1007/s00223-016-0168-9
7. Scheller EL, Doucette CR, Learman BS et al (2015) Region-specific variation in the properties of skeletal adipocytes reveals regulated and constitutive marrow adipose tissues. Nat Commun 6:7808. https://doi.org/10.1038/ncomms8808
8. Akintoye SO, Lam T, Shi S et al (2006) Skeletal site-specific characterization of orofacial and iliac crest human bone marrow stromal cells in same individuals. Bone 38:758–768. https://doi.org/10.1016/j.bone.2005.10.027
9. Kozloff KM, Volakis LI, Marini JC, Caird MS (2010) Near-infrared fluorescent probe traces bisphosphonate delivery and retention in vivo. J Bone Miner Res 25:1748–1758. https://doi.org/10.1002/jbmr.66
10. Yamada M, Matsuzaka T, Uetani M et al (1995) Normal age-related conversion of bone marrow in the mandible: MR imaging findings. Am J Roentgenol 165:1223–1228. https://doi.org/10.2214/ajr.165.5.7572508
11. Fazeli PK, Horowitz MC, MacDougald OA et al (2013) Marrow fat and bone—new perspectives. J Clin Endocrinol Metab 98:935–945. https://doi.org/10.1210/jc.2012-3634
12. Hardouin P, Rharass T, Lucas S (2016) Bone marrow adipose tissue: to be or not to be a typical adipose tissue?. Front Endocrinol 7:. https://doi.org/10.3389/fendo.2016.00085
13. Lips P, van Ginkel FC, Netelenbos JC (1985) Bone marrow and bone remodeling. Bone 6:343–344
14. Schwartz AV (2015) Marrow fat and bone: review of clinical findings. Bone Res 6:40. https://doi.org/10.3389/fendo.2015.00040
15. Patsch JM, Li X, Baum T et al (2013) Bone marrow fat composition as a novel imaging biomarker in postmenopausal women with prevalent fragility fractures. J Bone Miner Res 28:1721–1728. https://doi.org/10.1002/jbmr.1950
16. Devlin MJ (2013) Bone marrow composition, diabetes, and fracture risk: more bad news for saturated fat. J Bone Miner Res 28:1718–1720. https://doi.org/10.1002/jbmr.2013
17. Paccou J, Hardouin P, Cotten A et al (2015) The role of bone marrow fat in skeletal health: usefulness and perspectives for clinicians. J Clin Endocrinol Metab 100:3613–3621. https://doi.org/10.1210/jc.2015-2338
18. Pino AM, Miranda M, Figueroa C et al (2016) Qualitative aspects of bone marrow adiposity in osteoporosis. Front Endocrinol. https://doi.org/10.3389/fendo.2016.00139
19. Yeung DKW, Griffith JF, Antonio GE et al (2005) Osteoporosis is associated with increased marrow fat content and decreased marrow fat unsaturation: a proton MR spectroscopy study. J Magn Reson Imaging 22:279–285. https://doi.org/10.1002/jmri.20367
20. Naveiras O, Nardi V, Wenzel PL et al (2009) Bone-marrow adipocytes as negative regulators of the haematopoietic microenvironment. Nature 460:259–263. https://doi.org/10.1038/nature08099
21. Scheller EL, Cawthorn WP, Burr AA et al (2016) Marrow adipose tissue: trimming the fat. Trends Endocrinol Metab 27:392–403. https://doi.org/10.1016/j.tem.2016.03.016
22. Justesen J, Stenderup K, Ebbesen EN et al (2001) Adipocyte tissue volume in bone marrow is increased with aging and in patients with osteoporosis. Biogerontology 2:165–171
23. During A, Penel G, Hardouin P (2015) Understanding the local actions of lipids in bone physiology. Prog Lipid Res 59:126–146. https://doi.org/10.1016/j.plipres.2015.06.002
24. Mödder UI, Khosla S (2008) Skeletal stem/osteoprogenitor cells: current concepts, alternate hypotheses, and relationship to the bone remodeling compartment. J Cell Biochem 103:393–400. https://doi.org/10.1002/jcb.21423
25. Clabaut A, Delplace S, Chauveau C et al (2010) Human osteoblasts derived from mesenchymal stem cells express adipogenic

markers upon coculture with bone marrow adipocytes. Differentiation 80:40–45. https://doi.org/10.1016/j.diff.2010.04.004
26. Li M, Shen Y, Qi H, Wronski TJ (1996) Comparative study of skeletal response to estrogen depletion at red and yellow marrow sites in rats. Anat Rec 245:472–480. https://doi.org/10.1002/(SICI)1097-0185(199607)245:3<472::AID-AR3>3.0.CO;2-U
27. Du Z, Steck R, Doan N et al (2014) Estrogen deficiency associated bone loss in the maxilla: a methodology to quantify the changes in the maxillary intra-radicular alveolar bone in an ovariectomized rat osteoporosis model. Tissue Eng Part C Methods. https://doi.org/10.1089/ten.TEC.2014.0268
28. Jiao K, Dai J, Wang M-Q et al (2010) Age- and sex-related changes of mandibular condylar cartilage and subchondral bone: a histomorphometric and micro-CT study in rats. Arch Oral Biol 55:155–163. https://doi.org/10.1016/j.archoralbio.2009.11.012
29. Buie HR, Campbell GM, Klinck RJ et al (2007) Automatic segmentation of cortical and trabecular compartments based on a dual threshold technique for in vivo micro-CT bone analysis. Bone 41:505–515. https://doi.org/10.1016/j.bone.2007.07.007
30. Otsu N (1979) A threshold selection method from gray-level histograms. IEEE Trans Syst Man Cybern 9:62–66. https://doi.org/10.1109/TSMC.1979.4310076
31. Sengupta P (2013) The laboratory rat: relating its age with human's. Int J Prev Med 4:624–630
32. Sengupta S, Arshad M, Sharma S et al (2005) Attainment of peak bone mass and bone turnover rate in relation to estrous cycle, pregnancy and lactation in colony-bred Sprague–Dawley rats: suitability for studies on pathophysiology of bone and therapeutic measures for its management. J Steroid Biochem Mol Biol 94:421–429. https://doi.org/10.1016/j.jsbmb.2004.12.039
33. Johnston BD, Ward WE (2015) The ovariectomized rat as a model for studying alveolar bone loss in postmenopausal women. BioMed Res Int 2015:1–12. https://doi.org/10.1155/2015/635023
34. Kalu DN (1991) The ovariectomized rat model of postmenopausal bone loss. Bone Miner 15:175–191. https://doi.org/10.1016/0169-6009(91)90124-I
35. Lelovas PP, Xanthos TT, Thoma SE et al (2008) The laboratory rat as an animal model for osteoporosis research. Comp Med 58:424–430
36. Barngkgei I, Al Haffar I, Shaarani E et al (2016) Assessment of jawbone trabecular bone structure amongst osteoporotic women by cone-beam computed tomography: the OSTEOSYR project. J Investig Clin Dent 7:332–340. https://doi.org/10.1111/jicd.12170
37. Mavropoulos A, Rizzoli R, Ammann P (2007) Different responsiveness of alveolar and tibial bone to bone loss stimuli. J Bone Miner Res 22:403–410. https://doi.org/10.1359/jbmr.061208
38. Elovic RP, Hipp JA, Hayes WC (1995) Ovariectomy decreases the bone area fraction of the rat mandible. Calcif Tissue Int 56:305–310
39. Wronski TJ, Lowry PL, Walsh CC, Ignaszewski LA (1985) Skeletal alterations in ovariectomized rats. Calcif Tissue Int 37:324–328
40. Devlin H, Whelton C (2015) Can mandibular bone resorption predict hip fracture in elderly women? A systematic review of diagnostic test accuracy. Gerodontology 32:163–168. https://doi.org/10.1111/ger.12077
41. Hassani-Nejad A, Ahlqwist M, Hakeberg M, Jonasson G (2013) Mandibular trabecular bone as fracture indicator in 80-year-old men and women. Eur J Oral Sci 121:525–531. https://doi.org/10.1111/eos.12087
42. Mavropoulos A, Ammann P, Bresin A, Kiliaridis S (2005) Masticatory demands induce region-specific changes in mandibular bone density in growing rats. Angle Orthod 75:625–630. https://doi.org/10.1043/0003-3219(2005)75[625:MDIRCI]2.0.CO;2
43. Mavropoulos A, Ödman A, Ammann P, Kiliaridis S (2010) Rehabilitation of masticatory function improves the alveolar bone architecture of the mandible in adult rats. Bone 47:687–692. https://doi.org/10.1016/j.bone.2010.06.025
44. Allen MR (2011) The effects of bisphosphonates on jaw bone remodeling, tissue properties, and extraction healing. Odontology 99:8–17. https://doi.org/10.1007/s10266-010-0153-0
45. Choi DY, Sun KH, Won SY et al (2012) Trabecular bone ratio of the mandibular condyle according to the presence of teeth: a micro-CT study. Surg Radiol Anat 34:519–526. https://doi.org/10.1007/s00276-012-0943-x
46. van Eijden TMGJ., van der Helm PN, van Ruijven LJ, Mulder L (2006) Structural and mechanical properties of mandibular condylar bone. J Dent Res 85:33–37. https://doi.org/10.1177/154405910608500105
47. Bresin A, Kiliaridis S, Strid K-G (1999) Effect of masticatory function on the internal bone structure in the mandible of the growing rat. Eur J Oral Sci 107:35–44. https://doi.org/10.1046/j.0909-8836.1999.eos107107.x
48. Chappard D, Pascaretti-Grizon F, Gallois Y et al (2006) Medullar fat influences texture analysis of trabecular microarchitecture on X-ray radiographs. Eur J Radiol 58:404–410. https://doi.org/10.1016/j.ejrad.2005.12.033
49. Di Iorgi N, Rosol M, Mittelman SD, Gilsanz V (2008) Reciprocal relation between marrow adiposity and the amount of bone in the axial and appendicular skeleton of young adults. J Clin Endocrinol Metab 93:2281–2286. https://doi.org/10.1210/jc.2007-2691